



# Medical Implant Surface Technology: Geometrical Formation of Titania Nanotube Arrays by Divergence Anodization Parameters

Rabiatul Basria S. M. N. Mydin<sup>1</sup> · Roshasnorlyza Hazan<sup>2</sup> · Wan Nuramiera Wan Eddis Effendy<sup>1</sup> · Nur Afiqah Amalina Romli<sup>1</sup> · Sadiqah Shaharuddin<sup>3</sup> · Ibrahim Hussin Khan<sup>1</sup> · Srimala Sreekantan<sup>4</sup>

Received: 20 November 2022 / Revised: 13 June 2023 / Accepted: 8 July 2023 / Published online: 7 August 2023  
© The Author(s), under exclusive licence to Springer Nature Switzerland AG 2023

## Abstract

Titania nanotube arrays (TNA) offered great potential in medical implant surface technology. Anodization has been described as a cost-effective method to create highly ordered nano-porous oxide pores on the surface of the titanium surface. This work studied the growth behavior of TNA including anodization voltage, period, current density, and electrolyte aging condition with potential adherence profiles. This process was carried out at 30 V with a sweep rate of 1 V/s for different duration. The optimum geometrical formation of anatase TNA was successfully anodized at 30 V with a sweep rate of 1 V/s for 30 min using overnight aged electrolytes and supported by cellular adherence profiles. These investigations would provide beneficial knowledge on TNA geometrical advantages for biomedical applications.

**Keywords** Geometrical · Titania nanotube arrays · Anodization parameter · Surface technology · Medical implant · Nanosurface

## 1 Introduction

Titanium (Ti) presented a variety of unique characteristics which is applicable in many filed over the last 50 years [1] especially as implantable materials. A number of reports have shown that the surface structure of Ti is critical for determining the success or failure of clinical Ti implantation for the purpose of bone, joint, or tooth replacements [2–5]. In the past, numerous studies on implant surface modifications have been studied to optimize the surface geometry that best-fit cell interactions for adequate bone growth [6–8]. Recently efforts have been made to improve cell-stimulating,

biomimetic activities by designing new surface geometries at the nanoscale [9, 10].

Surface modification can be derived by transformation of structure, morphology and material surface composition without leaving the bulk mechanical properties. The aim of Ti surface modification is to produce a fine porous layer of biomaterials. Specifically, cavities and high surface area of precursor adsorption and anchoring were exploited [3, 11–13]. To further improve Ti bioactivity, biocompatibility, the interface between bone and implant, and implant anchorage to the bone, different surface modification methods have been explored. Typically, two different strategies have been developed. In the first approach by incorporating inorganic phases such as calcium phosphate on or into TiO<sub>2</sub> layer interface chemically was improved. In this inorganic chemical modification, bone regeneration is stimulated and biochemical interlocking between bone matrix proteins and surface materials increases. Conversely, biochemical surface modification is differed from the first strategy and refers to organic molecule incorporation such as protein, enzymes or peptides to persuade specific cell and tissue responses [14–19].

For the second approach, the interface is improved physically and geometrically by surface topography architecture. At the micrometer stage, a rough surface creates a higher

✉ Rabiatul Basria S. M. N. Mydin  
rabiatulbasria@usm.my

<sup>1</sup> Department of Biomedical Science, Universiti Sains Malaysia (USM), 13200 Kepala Batas, Pulau Pinang, Malaysia

<sup>2</sup> Materials Technology Group, Industrial Technology Division, Malaysian Nuclear Agency, Bangi, 43000 Kajang, Selangor Darul Ehsan, Malaysia

<sup>3</sup> School of Mechatronics Engineering, Universiti Malaysia Perlis, Pejabat Pos Besar, 01000 Kangar, Perlis, Malaysia

<sup>4</sup> School of Materials and Mineral Resources Engineering, 14300 Nibong Tebal, Pulau Pinang, Malaysia

surface area interaction rather than a smooth surface. This rough surface increases bone anchorage and reinforced the biomechanical interlocking of the implant with bone up till a certain level of roughness. At the nanometer stage, the roughness increases surface energy to improve protein matrix adsorption, bone cell migration, proliferation and osseointegration [17]. To date, anodization of Ti has been investigated because can easily create biological-inspired nanometer roughness. Therefore, optimized geometrical properties of an implant surface is crucial, especially on surface characteristic (e.g., chemistry, topography, surface energy and morphology [20–22].

In the past decade, Kubota have suggested that TiO<sub>2</sub> nanotube arrays grows on Ti metal would be the best candidate as an implant material. The excellent biocompatibility appears to depend on the presence of a passive oxide layer (TiO<sub>2</sub> layer) formed on the surface [23]. Several anodization variables such as voltage, anodization period, pH and temperature of electrolyte bath contribute to the TNA nanostructure formation [24]. Up to now, several generations of nanotubes have been brought forward [25, 26] to further improve its dimensionality. This work studied on the growth behavior of TNA including anodization voltage, period, current density, electrolytes aging condition with cellular adherence profiles. These investigations would provide beneficial knowledge on TNA geometrical advantages for biomedical applications.

## 2 Materials and Methods

### 2.1 Materials

The titanium (Ti) foil of 0.13 mm thickness with 99.7% purity was purchased from STREM Chemicals, USA. Prior use the foil was cleaned with acetone (Merck, USA) in ultrasonication for 15 min, then were rinsed with deionised water and dried at room temperature (RT). Ammonium fluorides (NH<sub>4</sub>F) salt were purchased from Merck, USA. The study materials were sterilised in 70% (v/v) ethanol followed by cleaning with sterile deionised water before introducing for autoclaving at 121 °C for 20 min.

### 2.2 Synthesis Parameters

Self-organised highly ordered TNA was successfully achieved by electrochemical anodization following the method by Effendy et al. [27, 29–32]. TNAs were prepared by electrochemical anodisation (EA) and monitored using Leios Material Analysis software. The pH of the electrolyte was maintained at pH 7 throughout the work. Anodic potential at 30 V with sweep rate of 1 V/s for different duration (10 s, 1 min, 2 min, 5 min, 10 min, 20 min, 30 min, 1 h, 2 h,

3 h and 6 h) was implemented in the whole process. The anodized sample was annealed to achieve the anatase crystalline phase as described previously [28–31].

### 2.3 Cell Cultures

Human osteoblast cell line SaOS-2 (HTB-85TM), human embryonic kidney cell line HEK 293 (ATCC CRL-1573), and human colon cancer cell line HT 29 (HT-29—HTB-38—ATCC) were all purchased from ATCC. Professor George Tsao of the University of Hong Kong provided HK-1, C666-1, meanwhile, was a gift from Professor Kwok-Wai Lo of the Faculty of Medicine, Department of Anatomical & Cellular Pathology, The Chinese University of Hong Kong. HEK 293 and HT 29 were maintained in DMEM supplemented with 1% (v/v) Penstrep, 1% (v/v) L-Glutamine, 10% (v/v) foetal bovine serum and 12.5 g/L of HEPES in a humidified incubator at 37 °C, 5% CO<sub>2</sub>. HK-1, C666-1 and SaOS-2 were maintained in a complete medium of RPMI with the same formulated supplements.  $1 \times 10^5$  cells were seeded on 1 cm × 1 cm TNA surface using a 24-well plate for 48 h culture period.

Prior to FESEM analysis, cells on the top side of TNA samples were fixed in a fixative agent. Briefly, the TNA samples were gently rinsed with PBS, thrice then subsequently treated with 2.5% (v/v) cold glutaraldehyde for half an hour. Then, all samples were rinsed once with PBS before dehydrating with increasing concentrations of ethanol (50, 70, 90 and 99% (v/v)) for 5-min per concentration. Each sample was separately stored at –20 °C before FESEM analysis was conducted. Gold palladium coating sputter was performed to improve the conductivity for clear and concise images. All experiments were performed in triplicate.

## 3 Results

### 3.1 The Electrolyte and Voltage Parameters

In general, anodisation voltage with 30 V produces between  $66.149 \pm 13.6$  to  $76.994 \pm 9.87$  of average TNA diameter. On the other hand, anodisation voltage with 60 V produces between  $121.752 \pm 18.5$  to  $169.53 \pm 14.6$  of average TNA diameter. Apart from voltage, the preparation of electrolytes and the growth of TNA was studied as shown in Fig. 1. Table 1 shows the average diameter of the TNA after anodization in electrolytes aged at different period. The longer the mixing period, the more soluble the fluoride salt, thereby making the release and uptake of ions easy for TNA growth. FESEM analysis of TNA in the electrolyte at 1 and 5 h shows the disorganised formation of TNA compared with TNA anodised in electrolyte aged overnight (16 h).

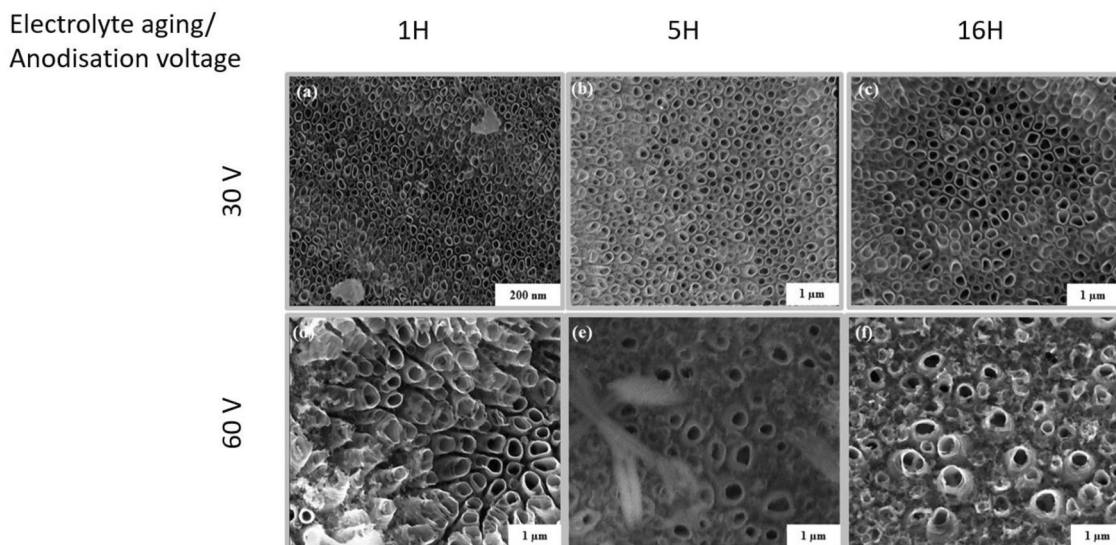


Fig. 1 FESEM images of TNA with different anodisation voltage and electrolyte aging buffers

Table 1 The average diameter of TNA in different anodisation voltage and electrolytes aging periods

Electrolyte aging (h)	Voltage (V)	Average diameter (nm)
1	30	66.149 ± 13.6
	60	154.39 ± 11.8
5	30	76.994 ± 9.87
	60	169.53 ± 14.6
16	30	72.517 ± 20.4
	60	121.752 ± 18.5

SD represent the triplicate experiment data

However, the electrolyte aging did not clearly influence by the anodisation voltage condition for TNA diameter.

### 3.2 Current Density

Furthermore, the typical current density recorded during anodization of Ti at 30 V in glycerol containing 0.5 wt% NH<sub>4</sub>F solution is displayed in Fig. 2. There is correlation between the current transient behaviour and changes in surface morphology of the oxide layer formed on Ti foil during anodization. As can be seen in Fig. 2, the current density decreased drastically from 1.8 to about 1.1 mA within first few minutes due to the formation of compact oxide layer.

Oxidation of Ti was according to the Eqs. 1–4. The electrode reaction was confirmed by formation of white bubble surrounding the cathode electrode at the beginning of anodization due to O<sub>2</sub> evolution. Details formation of the TNA

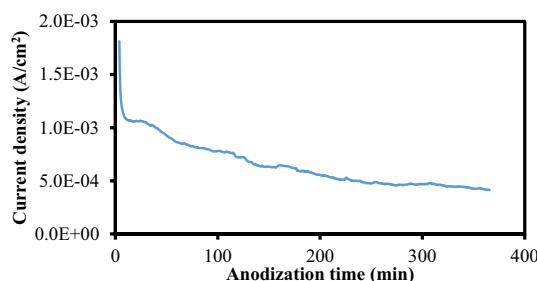
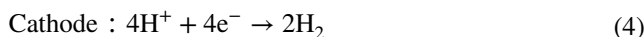
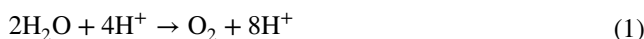


Fig. 2 Current density vs. time during anodization of Ti in glycerol containing 0.5 wt% NH<sub>4</sub>F solutions at 30 V

was been discussed concisely by Sreekantan et al. and Indira et al. [32, 33].



### 3.3 Anodization Duration

Figure 3 shows the formation of nanoporous oxide layer at different anodization duration. From Fig. 3b and c, random pits formation can be seen to take place up to 2 min. Interaction of surface Ti<sup>4+</sup> ions with oxygen ions in the electrolyte

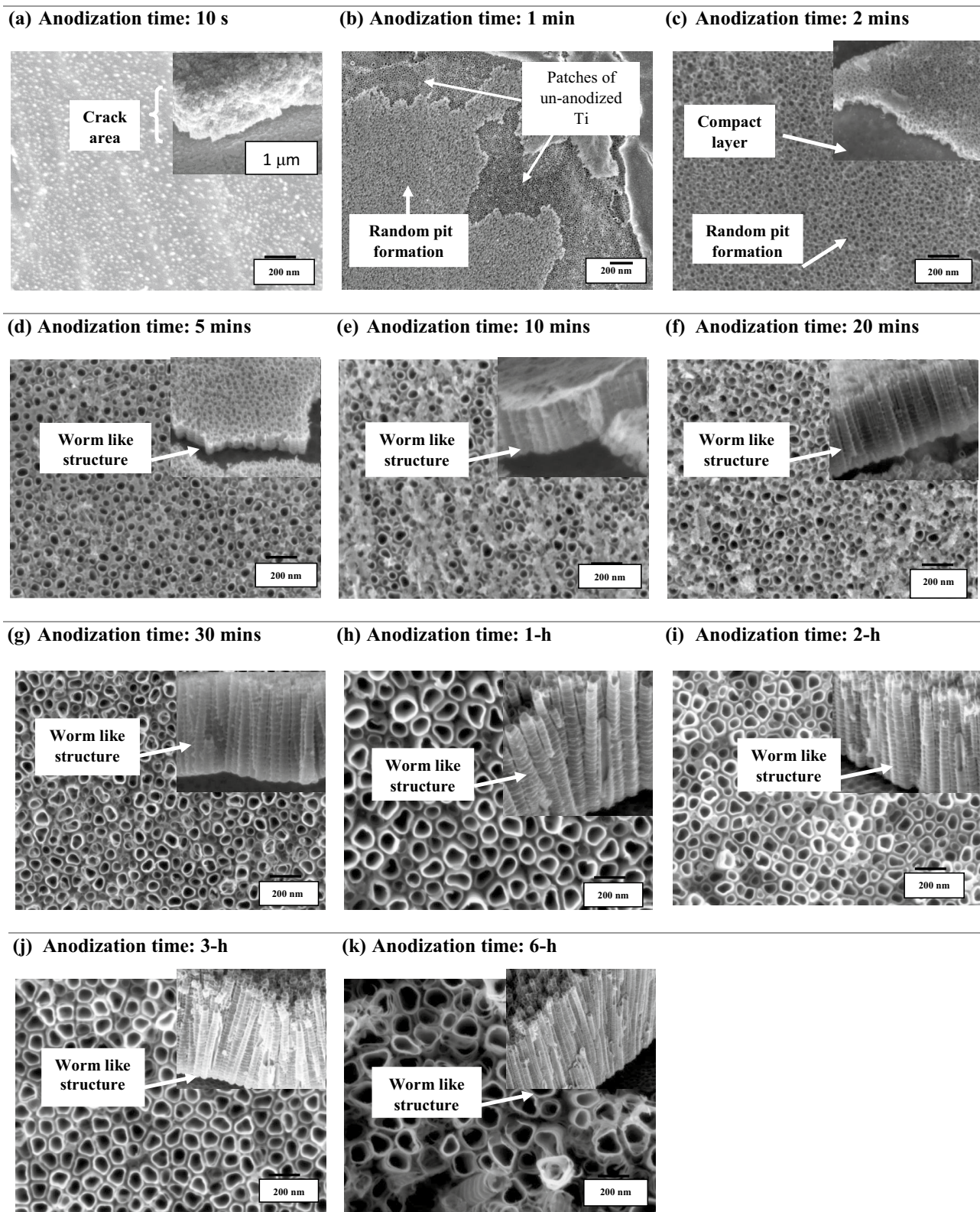
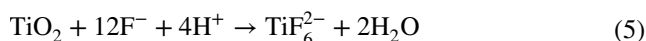


**Fig. 3** Evolution of the nano-tubular oxide layer during anodisation of Ti in glycerol+0.5 wt%  $\text{NH}_4\text{F}$  solutions at 30 V for **a** 10 s, **b** 1 min, **c** 2 min, **d** 5 min, **e** 10 min, **f** 20 min, **g** 30 min, **h** 1 h, **i** 2 h, **j** 3 h and **k** 6 h

formed an initial oxide layer during the first 10 s of anodization (Fig. 3a) and compact layer of TiO<sub>2</sub> formed on Ti foil can be seen. There were large cracked area of porous oxide film and craters at the interface film substrate could provide easy pathways for ions penetration from electrolyte. A few patches of un-anodized Ti still present after 1 min of anodization (Fig. 3b) and in (Fig. 3c), there is a complete transformation from Ti to TiO<sub>2</sub> porous layer on the sample surface after 2 min of anodization. The pores are not self-ordered at this stage and small pits that originated from localized oxide were observed due to the dissolution of the chemical process induced by F<sup>-</sup> ions where it acted as a pore-forming centre. Hence, the electrolyte ions will easily penetrate into the interface and form pores.

Anodization for 5 min (Fig. 3d) resulted in the separation of individual tubes from the nano-pores to larger pores where the thickness of outer oxide layer is about 225 nm. As time increase, distinct nanoporous morphology is observed (Fig. 3e) on the sample surface after 10 min of anodization. The breakdown sites act as seeds to disordered worm-like structure growth (Fig. 3e–k). The dissolution of TiO<sub>2</sub> from Ti resulted in pH gradient at top and bottom pore of the tube where lower pH could be accelerating the dissolution and pore penetration into Ti substrate resulted in pore transition from irregular to regular formation. To form uniform nanotube morphology, different pore will compete with each other for total available current and if the current is sufficient, the pore will survive and retain the morphology of the tube [34]. Small increase of current density around 30 min indicated the nucleation of nanopores and nanotubular oxide formation due to the random breakdown of barrier oxide film on Ti surface and dissolution of F<sup>-</sup> ions. Dissolution of TiO<sub>2</sub> to form pores occurred according to the Eq. 5.



The appearance of sample anodized for 20 min (Fig. 3f) was better than 10 min because the debris on anodized surface was less. Thus, it is clear that from 5 to 20 min, the pit transforms to tubular structure. However, compact oxide partially covering the surface. Clear self-ordered TNA structures could be observed after 30 min of anodization (Fig. 3g). The original oxide layer clearly dissolved. Anodization of Ti for 1 h, 2 h and 3 h (Fig. 3h–j) has similar morphology as sample anodized for 30 min. The TNA inner diameters were constant with time. However, by increasing the anodization time beyond 30 min, TNA length were found to increase [35]. At this stage, the predominant formation of the oxide layer is maintained, resulting in the formation of a thick oxide layer along with a slow chemical dissolution process. As the experiment continues, the chemical dissolution process actively proceeds according to Eqs. 1 and 2. Even though the length of TNA keeps increasing with time,

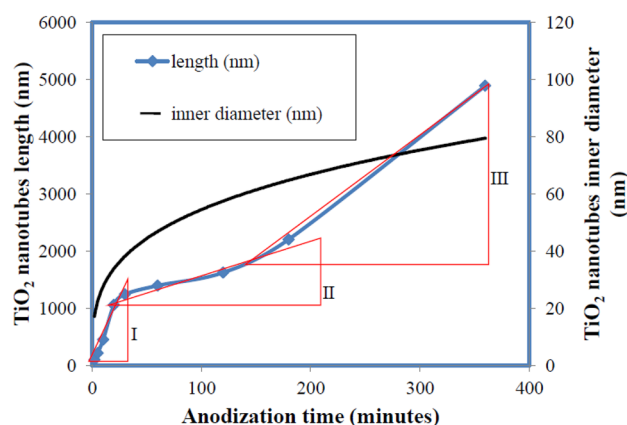


**Fig. 4** Correlation of TNA nanotubes length and inner diameter with regard of anodization time. The triangles indicate the growth rate of TNA nanotubes at three different stages indicate by stage I, II and III

**Table 2** Growth rate of TNA formation

Stages	Growth rate (nm/min)
I (0–30 min)	60.00
II (30 min–2 h)	4.44
III (2–6 h)	14.29

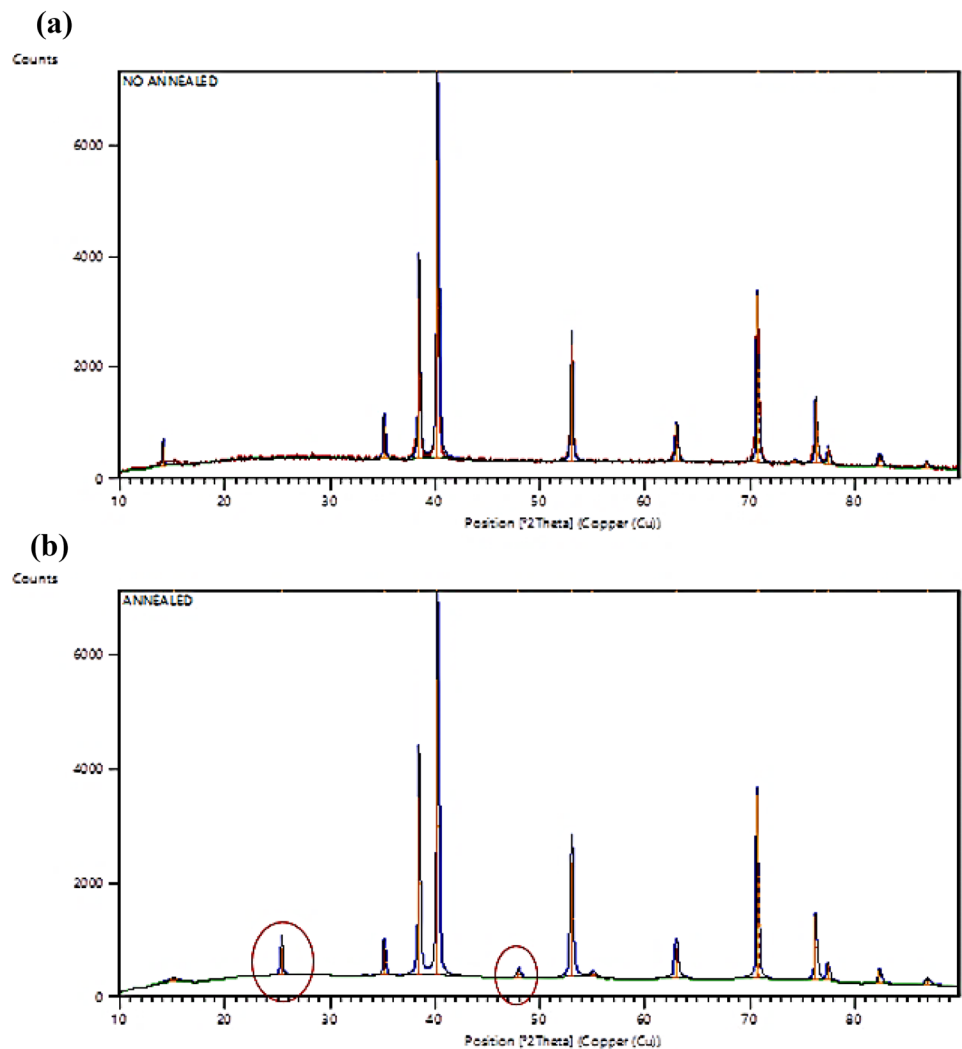
the TNA started to collapse and peel off from Ti foil after 6 h (Fig. 3k) of anodization. Therefore, anodization time need to fix within 30 min to 3 h to have adequate well-developed nanotubes.

Figure 4 show the correlation of TNA length and inner diameter with regard of anodization time. From the graph, the thickness of TNA porous layer was influenced by anodization time. It was noticed that three different stage of inner diameter growth rate. At early stage (stage I) of anodization (within 2 min to 30 min), the length of nanotubes drastically increased. Table 2 shows the growth rate of TNA formation. The growth rate was greatly decreased after 1 h to 2 h of anodization. The longest TNA was produced after 6 h of anodization. However, long TiO<sub>2</sub> nanotubes (~5 μm) tend to peel off. So, it is not suitable to be used for cell interaction studies. Therefore, TNA anodized for 3 h with 2.2 μm length was selected to undergo a cell interaction study.

### 3.4 The Crystalline Properties

Figure 5 showed XRD patterns recorded at room temperature of un-annealed TNA and annealed TNA noted as (a) and (b). The outcome of the analysis manifested smaller anatase crystal size of un-annealed compared to annealed TNA. Crystallite size of annealed TNA showed slight increase compared to un-annealed TNA. Two new

**Fig. 5** XRD analysis of un-annealed (A) and annealed (B) TNA



peaks were observed (red ring) showing crystalline of sample occurred at position 250 and 480. The anatase peak of TNA can be identified at 25.5, 38.5, 54.5 which correspond to (101), (004), (200), and (105), respectively.

### 3.5 FESEM Adhesion Profiles

The initial stages of cell adhesion are critical for bio-material integration. Therefore, in the present study, the adherence response of various human cell line models on TNA was studied using FESEM. The cellular protrusion adheres on the nanotube's surface as shown in Fig. 6a–e. Detailed observation found possible filopodia interaction with the nanosurface as indicated by the red and yellow arrows. Figure 6a, c, d, and e showed clear cell spreading and proliferation activities (indicated by cell numbers).

## 4 Discussion

Presently, arrays consisting of highly ordered TNA fabricated by a simple electrochemical approach have attracted more researchers [36–38] to participate in this research area. Several factors have been discussed affecting the geometry of TNA formation [39–43]. Therefore, this work described in detail on the electrolyte, voltage, current density, anodization duration, and crystal structure of TNA-associated respective geometrical properties.

There are three possible major reactions depending on anodization parameters involving electrolytes condition; first is the formation of the metal ions ( $Mn^+$ ) from dissolving the metal in the solution, second is metal oxide formation due to the interaction of metal ions with oxygen ions from water molecules in the electrolyte and this metal

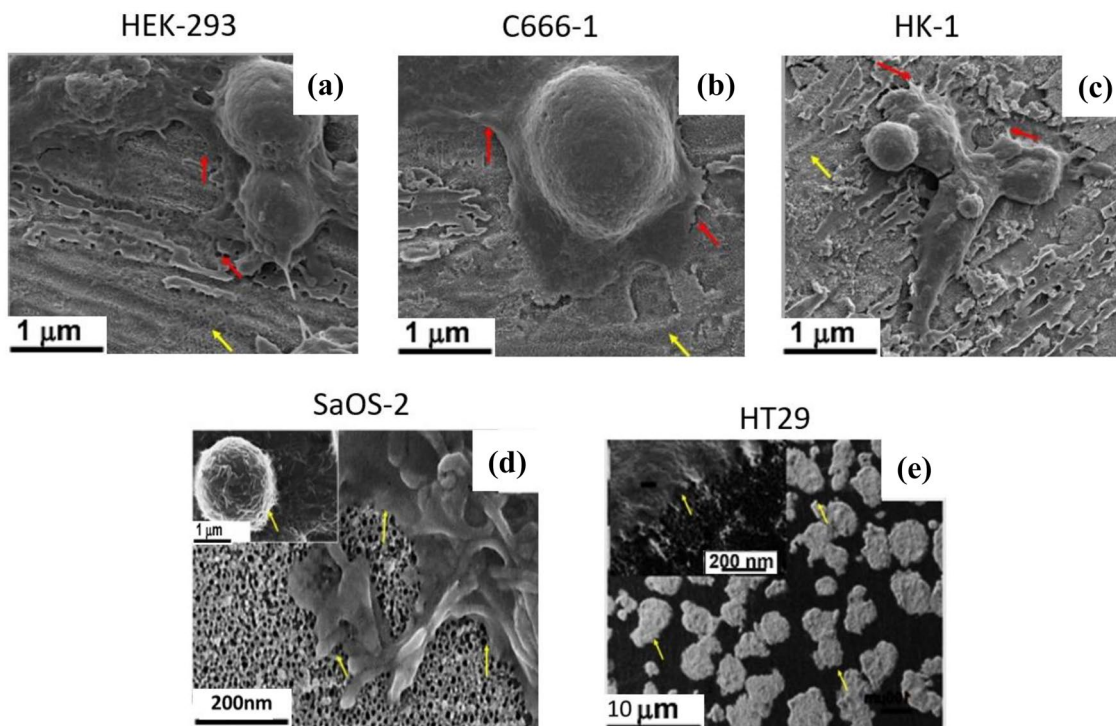


**Fig. 6** Cells attachment studies on TNA surface by FESEM. The yellow arrow indicates the presence of filopodia anchoring the TNA surfaces

oxide can be found on the surface in the bulk layer where the metal oxide products are insoluble in the electrolyte, lastly is oxide formation and oxide dissolution reactions in specific conditions will compete with each other to form porous in the metal oxide layer [44].

Findings from this study found that the electrolyte aging did not clearly influence the anodisation voltage for TNA formation. However, aged electrolytes could lead to better TNA growth. It is clear that the anodizing voltage has an important effect on the anodization of Ti. Gulati et al. [23] discovered the benefit of applying recycled, aged electrolytes, which improved the topography of the TNA and resulted in a smoother surface. Based on the result from Fig. 3, we can identify two basic mechanisms to form nanoporous structures; (1) electrochemical oxidation and (2) chemical dissolution. An initial  $\text{TiO}_2$  layer or barrier layer is formed on a metal surface under the application of an electric field. Then pore initiation occurred in the presence of fluoride ( $\text{F}^-$ ) ions at preferred sites on the oxide layer due to electric field-assisted dissolution. These oxidation and chemical dissolutions were active at the pore bottom. The barrier layer was reduced by pore formation while concentrated electric field intensity beneath the barrier layer ensures further growth of pores [45].

In this study, the anodic parameters of 30 V with a sweep rate of 1 V/s for 30 min produce well-aligned TNA on the oxide layer. In general, regular nanotubes were formed in

shorter duration of anodization and irregular nanotubes were formed in longer duration of anodization as a result of excessive dissolution occurring along the whole tube length. Previous studies reported that the length of the nanotubes increases dramatically by extending anodization reaction time. The oxide-growth process at the  $\text{TiO}_2$  nanotubes bottom and the oxide-dissolution process at the  $\text{TiO}_2$  nanotubes mouth are two important processes responsible for the nanotubes anodic growth. The  $\text{TiO}_2$  nanotube length increases gradually before the dissolution rate becomes equal to the  $\text{TiO}_2$  nanotube growth rate.

From the graph in Fig. 4, the growth rate TNA was detected at three different regions. At stage I,  $\text{TiO}_2$  dissolution at the bottom of the pits was accelerated making the barrier layer at the bottom relatively thin [46]. In turn, the electric field intensity increases resulting in further pore growth. In meanwhile, electrochemical etching by  $\text{F}^-$  ions also takes place and converts the tubes into larger tubes. It can be seen that TNA formation became slower at the second 2 stage. It is because the  $\text{F}^-$  became less for electrochemical to take place and not much changes in  $\text{TiO}_2$  nanotubes inner diameter. The TNA formation growth rate decreases due to the equal rate of chemical dissolution and electrochemical etching at stage II. At the final stage (stage III), TNA inner diameter hardly varied because electrochemical etching was slower than in stage 2. It is due to the absence of  $\text{F}^-$  ion. Thus, the chemical dissolution suppresses the

electrochemical etching resulting higher rate of TNA length growth.

The outcome from this study found smaller anatase crystal size of un-annealed compared to annealed TNA. The crystallite size of annealed TNA showed a slight increase compared to unannealed TNA. The crystalline phase of TNA plays a crucial point in promoting cell interaction to the nanosurface [46]. Lai et al. [47] mentioned that anatase phase TNA can be achieved at 400 °C for 2-h which had been applied in our work. The predominant anatase phase was seen on the sample treated at 400 °C compared to the un-annealed sample. In the reports by Yu et al., the crystallinity of TNA also influenced cell adhesion [48, 49].

Anatase phase TNA is more biocompatible than amorphous TNA due to changes in wettability and surface energy [50, 51]. The properties of the TNA surface in promoting cell attachment are studied, such as the presence of gas during the annealing stage. Argon gas enhances the surface energy of the TNA nanosurface [52, 53] to become more positive, thereby attracting the negatively charged cells to fix and proliferate on the TNA surface compared with normal air. However, the main idea of cells attached to the nanosurface was due to the roughness of the TNA surface [54]. TNA growth promotes a larger surface area, providing space for cell attachment and filopodia anchoring. The cell structure is also maintained during cell proliferation, which supports the idea of TNA as a biocompatible material, particularly in implantation [55].

Further observation via FESEM and supported by our previous work on cellular interaction on TNA found various cellular protrusion activities on the surface of the nanotubes which mediates cell adhesion and provides a cell survival signal [56–59]. Adherence and spread of cells cultured on TNA might be due to the extremely larger surface area, the distinct up-and-down vertical topography contributing to the locked-in cell arrangement, and the existence of the body fluid channel in-between TiO<sub>2</sub> nanotubes. These interactions might involve mechano-cytoskeleton remodeling activities as described in previous work [60, 61]. Previous works [62, 63] also supported that stated that cells that stretched on a material surface with more anchorage could provide good adhesion properties that are curial for medical implant surface technology.

## 5 Conclusion

The geometrical formation of TNA by anodization is directly affected by the electrolyte aging condition, anodization duration, and crystal structures. In this study, the anodic potential of TNA was successfully maintained at 30 V with a sweep rate of 1 V/s for 30 min, and the structure of TNA was well aligned on the oxide layer. The TNA geometrical advantages

may provide better cellular adhesion profiles that beneficial for medical implant surface technology.

**Author Contributions** RBSMNM involved in the conceptualization, manuscript writing, reviewing the finding related to the systematic review and funding acquisition. WNWEE contributed on the data collecting, analysis, and draft writing. RH contributed in the initial idea of the work and data analysis. NAAR, SS and IHK contributed in the data collection. SS involved in reviewing and funding acquisition. All authors reviewed the manuscript.

**Funding** The authors wish to thank Universiti Sains Malaysia for funding this works with research Grants; RUI EKSESAIS 2019 (No:1001/CIPPT/8012338) for sponsoring this work.

**Data availability** The availability of data as attached in the file.

## Declarations

**Conflict of interest** All author declared that there is no conflict of interest.

**Ethical approval** The authors declared no experiment conducted unethically.

## References

- Peng Z, Ni J (2019) Surface properties and bioactivity of TiO<sub>2</sub> nanotube array prepared by two-step anodic oxidation for biomedical applications. *R Soc Open Sci* 6(4):181948
- Mishnaevsky L Jr, Levashov E, Valiev RZ, Segurado J, Sabirov I, Enikeev N, Prokoshkin S, Solovoyov AV, Korotitskiy A, Gutmanas E, Gotman I (2014) Nanostructured titanium-based materials for medical implants: modeling and development. *Mater Sci Eng R Rep* 81:1–19
- Losic D (2021) Advancing of titanium medical implants by surface engineering: recent progress and challenges. *Expert Opin Drug Deliv* 18(10):1355–1378
- van Hove RP, Sierevelt IN, van Royen BJ, Nolte PA (2015) Titanium-nitride coating of orthopaedic implants: a review of the literature. *BioMed Res Int* 2015:485975
- Lin L, Wang H, Ni M, Rui Y, Cheng TY, Cheng CK, Lin C (2014) Enhanced osteointegration of medical titanium implant with surface modifications in micro/nanoscale structures. *J Orthopaed Transl* 2(1):35–42
- Roguska A, Pisarek M, Belcarz A, Marcon L, Holdynski M, Andrzejczuk M, Janik-Czachor M (2016) Improvement of the bio-functional properties of TiO<sub>2</sub> nanotubes. *Appl Surf Sci* 388:775–785
- Vasilev K, Poh Z, Kant K, Chan J, Michelmores A, Losic D (2010) Tailoring the surface functionalities of titania nanotube arrays. *Biomaterials* 31(3):532–540
- Su EP, Justin DF, Pratt CR, Sarin VK, Nguyen VS, Oh S, Jin S (2018) Effects of titanium nanotubes on the osseointegration, cell differentiation, mineralisation and antibacterial properties of orthopaedic implant surfaces. *Bone Joint J* 100(1):9–16
- Souza JC, Sordi MB, Kanazawa M, Ravindran S, Henriques B, Silva FS, Cooper LF (2019) Nano-scale modification of titanium implant surfaces to enhance osseointegration. *Acta Biomater* 94:112–131



10. Park J, Bauer S, von der Mark K, Schmuki P (2007) Nanosize and vitality: TiO<sub>2</sub> nanotube diameter directs cell fate. *Nano Lett* 7(6):1686–1691
11. Brammer KS, Frandsen CJ, Jin S (2012) TiO<sub>2</sub> nanotubes for bone regeneration. *Trends Biotechnol* 30(6):315–322
12. Parcharoen Y, Termsuksawad P, Sirivisoot S (2016) Improved bonding strength of hydroxyapatite on titanium dioxide nanotube arrays following alkaline pretreatment for orthopedic implants. *J Nanomater* 2016:1–16
13. Ahn TK, Lee DH, Kim TS, Jang GC, Choi S, Oh JB, Ye G, Lee S (2018) Modification of titanium implant and titanium dioxide for bone tissue engineering. In: Chun HJ, Park K, Kim CH, Khang G (eds) *Novel biomaterials for regenerative medicine*. Springer, Singapore, pp 355–368
14. Bhattarai DP, Shrestha S, Shrestha BK, Park CH, Kim CS (2018) A controlled surface geometry of polyaniline doped titania nanotubes biointerface for accelerating MC3T3-E1 cells growth in bone tissue engineering. *Chem Eng J* 350:57–68
15. Simi VS, Mohan L, Rajendran N (2021) Tailoring the surface functionalities of titania nanotubes for biomedical applications. *Nanomaterials and their biomedical applications*. Springer, Singapore, pp 513–552
16. Brammer KS, Oh S, Cobb CJ, Bjursten LM, van der Heyde H, Jin S (2009) Improved bone-forming functionality on diameter-controlled TiO<sub>2</sub> nanotube surface. *Acta Biomater* 5(8):3215–3223
17. Skoog SA, Kumar G, Narayan RJ, Goering PL (2018) Biological responses to immobilized microscale and nanoscale surface topographies. *Pharmacol Ther* 182:33–55
18. Wu S, Weng Z, Liu X, Yeung KWK, Chu PK (2014) Functionalized TiO<sub>2</sub> based nanomaterials for biomedical applications. *Adv Funct Mater* 24(35):5464–5481
19. Fox KE, Tran NL, Nguyen TA, Nguyen TT, Tran PA (2019) Surface modification of medical devices at nanoscale: recent development and translational perspectives. In: Yang L, Bhaduri S, Webster TJ (eds) *Biomaterials in translational medicine*. Academic Press, Cambridge, pp 163–189
20. Jeon H, Simon CG Jr, Kim G (2014) A mini-review: cell response to microscale, nanoscale, and hierarchical patterning of surface structure. *J Biomed Mater Res B Appl Biomater* 102(7):1580–1594
21. Variola F, Brunski JB, Orsini G, de Oliveira PT, Wazen R, Nanci A (2011) Nanoscale surface modifications of medically relevant metals: state-of-the-art and perspectives. *Nanoscale* 3(2):335–353
22. Mendonça G, Mendonça DB, Aragao FJ, Cooper LF (2008) Advancing dental implant surface technology—from micron-to nanotopography. *Biomaterials* 29(28):3822–3835
23. Gulati K, Maher S, Findlay DM, Losic D (2016) Titania nanotubes for orchestrating osteogenesis at the bone–implant interface. *Nanomedicine* 11(14):1847–1864
24. Capellato P, Vasconcelos LV, Vilela FB, Ribeiro GC, Correia CA, Silva G, Sachs D, Rangel AL, Zavaglia CAD, Claro AP (2021) Titanium-tantalum alloy surface modification by hydroxyapatite layer on TiO<sub>2</sub> nanotubes: effect on microbial activity. *Mater Res* 24:e20210285
25. Brammer KS, Oh S, Frandsen CJ, Jin S (2011) Biomaterials and biotechnology schemes utilizing TiO<sub>2</sub> nanotube arrays. *Biomater Sci Eng* 2011:193–210
26. Souza JC, Sordi MB, Kanazawa M, Ravindran S, Henriques B, Silva FS, Aparicio C, Cooper LF (2019) Nano-scale modification of titanium implant surfaces to enhance osseointegration. *Acta Biomater* 94:112–131
27. Effendy WNFWE, Mydin RBS, Gazzali AM, Sreekantan S (2020) Therapeutic nano-device: study of biopolymer coating on titania nanotubes array loaded with chemodrug targeted for localized cancer therapy application. *IOP Conf Ser* 932(1):012116
28. Mydin SMN, Sreekantan S, Hazan R, Farid Wajidi MF, Mat I (2017) Cellular homeostasis and antioxidant response in epithelial HT29 cells on titania nanotube arrays surface. *Oxid Med Cell Longev* 2017:1–10
29. Effendy WNFWE, Mydin SMN, Shanker K, Ng KY, Sundaraju P, Gunasagaran S, Ahmad Sopian SF, Mohd Gazzali A (2022) Comparative dose-and time-dependent manner of resveratrol on human epithelial cell types. *Rev Bras* 32(3):466–471
30. Effendy WNFWE, Mydin RBS, Sreekantan S, Sopian SFA, Sundaraju P, Gunasagaran S, Gazzali AM (2021) Titania nanotube arrays nanosystem for therapeutic delivery of resveratrol on neuronal cell lines model. *Malays J Med Health Sci* 17:7–14
31. Effendy WNFWE, Mydin RBS, Gazzali AM, Sreekantan S (2023) Localised delivery of cisplatin from chitosan-coated titania nanotube array nanosystems targeting nasopharyngeal carcinoma. *Adv Pharma Bull* 13(1):104
32. Sreekantan S, Lockman Z, Hazan R, Tasbihi M, Tong LK, Mohamed AR (2009) Influence of electrolyte pH on TiO<sub>2</sub> nanotube formation by Ti anodization. *J Alloys Compd* 485(1–2):478–483
33. Indira K (2015) Development of titanium nanotube arrays for orthopaedic applications. *Thesis*. <http://hdl.handle.net/10603/37614>. Accessed 3 Apr 2021
34. Shokuhfar T, Hamlekhan A, Chang JY, Choi CK, Sukotjo C, Friedrich C (2014) Biophysical evaluation of cells on nanotubular surfaces: the effects of atomic ordering and chemistry. *Int J Nanomed* 9:3737–3748
35. Luo B, Yang H, Liu S, Fu W, Sun P, Yuan M, Zhang Y, Liu Z (2008) Fabrication and characterization of self-organized mixed oxide nanotube arrays by electrochemical anodization of Ti–6Al–4V alloy. *Mater Lett* 62(30):4512–4515
36. Velasco-Ortega E, Ortiz-García I, Jiménez-Guerra A, Monsalve-Guil L, Muñoz-Guzón F, Perez RA, Gil FJ (2019) Comparison between sandblasted acid-etched and oxidized titanium dental implants: in vivo study. *Int J Mol Sci* 20(13):3267
37. Anwar T, Li W, Hussain N, Chen W, Sagar RUR, Tongxiang L (2016) Effect of annealing atmosphere induced crystallite size changes on the electrochemical properties of TiO<sub>2</sub> nanotubes arrays. *J Electr Eng* 4:43–51
38. Dale GR, Hamilton JWW, Dunlop PSM, Lemoine P, Byrne JA (2009) Electrochemical growth of titanium oxide nanotubes: the effect of surface roughness and applied potential. *J Nanosci Nanotechnol* 9(7):4215–4219
39. Moriai K, Nakajima N, Moriyoshi C, Maruyama H (2017) Synthesis of TiO<sub>2</sub> nanotubes: effect of post-treatment on crystallinity and photocatalytic activity. *Mater Res Express* 4(4):045017
40. Sudha D, Suganya R, Revathi A, Yoghaananthan K, Sivaprakash V (2022) Anodization of TiO<sub>2</sub> nanotubes on titanium alloys and their analysis of mechanical properties. *Mater Sci Forum* 1070:127–132
41. Khudhair D, Bhatti A, Li Y, Hamedani HA, Garmestani H, Hodgson P, Nahavandi S (2016) Anodization parameters influencing the morphology and electrical properties of TiO<sub>2</sub> nanotubes for living cell interfacing and investigations. *Mater Sci Eng C* 59:1125–1142
42. Liu G, Du K, Wang K (2016) Surface wettability of TiO<sub>2</sub> nanotube arrays prepared by electrochemical anodization. *Appl Surf Sci* 388:313–320
43. Khrunyk YY, Belikov SV, Tsurkan MV, Vyalykh IV, Markaryan AY, Karabanalov MS, Wysokowski M (2020) Surface-dependent osteoblasts response to TiO<sub>2</sub> nanotubes of different crystallinity. *Nanomaterials* 10(2):320
44. Jedi-soltanabadi Z, Pishkar N, Ghoranneviss M (2018) Enhanced physical properties of the anodic TiO<sub>2</sub> nanotubes via proper anodization time. *J Theoret Appl Phys* 12:135–139
45. Benčina M, Iglič A, Mozetič M et al (2020) Crystallized TiO<sub>2</sub> nanosurfaces in biomedical applications. *Nanomaterials* 10:1121

46. Lai CW, Sreekantan S (2011) Effect of applied potential on the formation of self-organized TiO<sub>2</sub> nanotube arrays and its photo-electrochemical response. *J Nanomater* 2011:11–11
47. Zhao JH, Michalski WP, Williams C, Li L, Xu HS, Lamb PR, Jones S, Zhou YM, Dai XJ (2011) Controlling cell growth on titanium by surface functionalization of heptylamine using a novel combined plasma polymerization mode. *J Biomed Mater Res Part A* 97(2):127–134
48. Daniel M, Eleršič Filipič K, Filová E, Judl T, Fojt J (2023) Modelling the role of membrane mechanics in cell adhesion on titanium oxide nanotubes. *Comput Methods Biomech Biomed Eng* 26(3):281–290
49. Wawrzyniak J, Karczewski J, Kupracz P, Grochowska K, Coy E, Mazikowski A, Ryl J, Siuzdak K (2020) Formation of the hollow nanopillar arrays through the laser-induced transformation of TiO<sub>2</sub> nanotubes. *Sci Rep* 10(1):20235
50. Lai Y, Huang J, Cui Z, Ge M, Zhang KQ, Chen Z, Chi L (2016) Recent advances in TiO<sub>2</sub>-based nanostructured surfaces with controllable wettability and adhesion. *Small* 12(16):2203–2224
51. Sul YT, Johansson CB, Jeong Y, Röser K, Wennerberg A, Albrektsson T (2001) Oxidized implants and their influence on the bone response. *J Mater Sci - Mater Med* 12:1025–1031
52. Manivasagam VK, Sabino RM, Kantam P, Popat KC (2021) Surface modification strategies to improve titanium hemocompatibility: a comprehensive review. *Mater Adv* 2(18):5824–5842
53. Huang JY, Lai YK (2015) TiO<sub>2</sub>-based surfaces with special wettability—from nature to biomimetic application. In: *Wetting and wettability*
54. Tian A, Qin X, Wu A, Zhang H, Xu Q, Xing D, Yang H, Qiu B, Xue X, Zhang D, Dong C (2015) Nanoscale TiO<sub>2</sub> nanotubes govern the biological behavior of human glioma and osteosarcoma cells. *Int J Nanomed* 10:2423–2439
55. Mydin RBS, Sreekantan S, Hazan R, Qazem EQ, Wajidi MFF (2019) Mechanosensitivity response of epithelial HT29 cells on titanium dioxide nanotube array surface via CK8 protein expression. *Int J Nano Biomater* 8(2):118–128
56. Mydin RBS, Wajidi MFF, Hazan R, Sreekantan S (2017) Nanobiointerface of titania nanotube arrays surface influence epithelial HT29 cells. *Trans Sci Technol* 4:348–353
57. Mydin RBS, Sreekantan S, Widera D, Saharudin KA, Hazan R, Wajidi MFF (2022) Genome-nanosurface interaction of titania nanotube arrays: evaluation of telomere, telomerase and NF-κB activities on an epithelial cell model. *RSC Adv* 12(4):2237–2245
58. Mydin RBS, Mahboob A, Sreekantan S, Saharudin KA, Qazem EQ, Hazan R, Wajidi MFF (2023) Mechano-cytoskeleton remodeling mechanism and molecular docking studies on nanosurface technology: titania nanotube arrays. *Biotechnol Appl Biochem* 70:1072
59. Palaniyappan K, Mydin SMN, Widera D, Noordin SS, Harun NH, Wan Eddis Effendy WN, Hazan R, Sreekantan S (2023) Double-edged sword of biofouling potentials associated with haemocompatibility behaviour: titania nanotube arrays for medical implant surface technology. *Beni-Suef Univ J Basic Appl Sci* 12(1):1–12
60. Hussein N, Mydin RBS, Effendy WNFWE, Mohd Gazzali A, Saharudin KA, Sreekantan S (2023) Titania nanotube arrays as nanobiomatrix interfaces for localized biomolecules delivery to human neuroblastoma SH-SY5Y cells. *Int Nano Lett* 13(2):155–163
61. Jemat A, Ghazali MJ, Razali M, Otsuka Y (2015) Surface modifications and their effects on titanium dental implants. *BioMed Res Int* 2015:791725
62. Cai S, Wu C, Yang W, Liang W, Yu H, Liu L (2020) Recent advance in surface modification for regulating cell adhesion and behaviors. *Nanotechnol Rev* 9(1):971–989
63. Effendy WNFWE, Mydin RBSMN, Sreekantan S, Gazzali AM, Musa MY (2023) Cisplatin encapsulation efficiency profiles using titania nanotube arrays platform in targeted cancer therapy. *Biointerface Res Appl Chem* 13(3):255–266

**Publisher's Note** Springer Nature remains neutral with regard to jurisdictional claims in published maps and institutional affiliations.

Springer Nature or its licensor (e.g. a society or other partner) holds exclusive rights to this article under a publishing agreement with the author(s) or other rightsholder(s); author self-archiving of the accepted manuscript version of this article is solely governed by the terms of such publishing agreement and applicable law.